Catalysis Science & Technology

PAPER

View Article Online
View Journal | View Issue



Cite this: *Catal. Sci. Technol.*, 2014, 4, 814

# $Ce_{1-x}Sm_xO_{1.9-\delta}$ nanoparticles obtained by microwave-assisted hydrothermal processing: an efficient application for catalytic oxidation of α-bisabolol

A. G. M. Silva,[a] T. S. Rodrigues,[a] A. Dias,[a] H. V. Fajardo,[a] R. F. Gonçalves,[b] M. Godinho[b] and P. A. Robles-Dutenhefner*[c]

Received 9th October 2013,
Accepted 21st December 2013

DOI: 10.1039/c3cy00788j

www.rsc.org/catalysis

Heterogeneous catalysts based on Sm-doped ceria were employed for the first time in the liquid-phase oxidation of α-bisabolol. Nanometer-sized catalysts were obtained by microwave-hydrothermal synthesis and were characterized by X-ray diffraction (XRD), temperature programmed reduction (TPR), Raman spectroscopy and $N_2$-physisorption. The influence of Sm doping, temperature and the solvent used on the catalytic behavior was investigated. Conversions up to 84% and a combined selectivity for the products up to 77% were obtained for $Ce_{0.9}Sm_{0.15}O_{1.85-\delta}$ catalysts. The reactions were highly selective for the epoxidation products (only bisabolol oxides A and B were obtained) and shown to be strongly dependent on the temperature and solvent employed. Best results were achieved for higher Sm concentrations, which indicate that changes in the textural properties due to doping produced a significantly more active catalyst.

## 1. Introduction

The functionalization of alcohols is a significant reaction in the fine chemicals field because they are useful precursors for the synthesis of important structures in organic chemistry, such as aldehydes, ketones, carboxylic acids and cyclic ethers.[1] Bisabolol is a sesquiterpene alcohol, which can be found in the essentials oils of cabreuva, candle and others. Their oxygenated derivatives, bisabolol oxides A and B, have major organoleptic properties, such as soft floral scents. They can be found in the essential oils of chamomile in low concentrations (lower than 2 wt%) and are widely used in the formulation of lotions, creams and cosmetics.[2,3] In the literature, work on the oxidation processes of α-bisabolol are all non-catalytic reactions employing biotransformation methods and vanadium complexes towards the epoxidation of homoallylic alcohols.[4–6]

Among the heterogeneous catalysts commonly employed in organic synthetic processes, $CeO_2$ (ceria) is widely recognized because of its excellent oxidation–reduction potential.[7–9] This catalyst and many doped derivatives can be produced by environmentally friendly methods, such as microwave-hydrothermal synthesis,[10,11] which can produce catalysts with tailor-made properties, such as high oxygen mobility, controlled porosity, nanometer-sized particles (3–10 nm), and high surface areas.[12–15] These properties are crucial for applications in catalyzed oxidation reactions, which can be further improved by doping $CeO_2$ catalysts with rare-earth oxides, resulting in non-stoichiometric ceria.[16]

Despite the low usage of α-bisabolol, its structural features favor the development of synthetic routes to obtain products with pharmacological activities, particularly molecules that contain cyclic ethers such as tetrahydrofuran and tetrahydropyran derivatives resulting in the bisabolol oxides A and B. In this context, we report a novel, efficient application for Sm-doped $CeO_2$ obtained by a microwave-hydrothermal method as heterogeneous catalysts in the oxidation of α-bisabolol. The catalytic behavior was evaluated in terms of their conversion and selectivity for the epoxidation products as functions of temperature and the solvent employed. To the best of our knowledge, the present work reports for the first time the use of heterogeneous catalysts in the oxidation of α-bisabolol towards a new, environmentally friendly route for this process.

## 2. Experimental

### 2.1. Catalyst preparation and characterization

The catalysts $Ce_{1-x}Sm_xO_{1.9-\delta}$ were prepared by a microwave-assisted hydrothermal method. Aqueous solutions were

[a] *Departamento de Química, Universidade Federal de Ouro Preto, Morro do Cruzeiro, 35400-00, Ouro Preto, MG, Brazil*
[b] *Departamento de Química, Universidade Federal de Goiás, CAC/UFG, Catalão, GO, Brazil*
[c] *Departamento de Química, ICEX, Universidade Federal de Minas Gerais, Av. Antônio Carlos, 6627, Pampulha, Belo Horizonte, MG, 31270-901, Brazil. E-mail: pard@ufmg.br*

prepared by mixing $Ce(NO_3)_3{\cdot}6H_2O$ (99.9%, Aldrich) and $Sm_2O_3$ (99.9%, Aldrich), previously solubilized in nitric acid, under stirring. Ammonium hydroxide was slowly added to complete the precipitation under a controlled pH. The resulting gel was then transferred to polytetrafluoroethylene (PTFE) vessels, reaching approximately 50% of the total volume, and heat treated in the microwave-assisted hydrothermal system (2.45 GHz and 800 W) at 130 °C (3 bar) for 20 min.

Powder X-ray diffraction (XRD) measurements were conducted for pre-dried samples (110 °C for 12 h) by using a Rigaku D-Max 2500a with Cu Kα radiation (40 kV, 40 mA, $\lambda$ = 0.15418 nm). The diffraction patterns were measured in the range 10–50° 2$\theta$ with a step size of 0.05° 2$\theta$ and a step time of 4.0 s. The reducibility of the catalyst surfaces was determined by Temperature-Programmed Reduction (TPR) using a Quantachrome instrument (ChemBET-300) equipped with a thermal conductivity detector. Prior to each analysis, *ca.* 150 mg was packed into a quartz cell, heated for 2 h at 200 °C under a helium stream, and then cooled to room temperature. The experiments were performed between 30 and 900 °C in a 5% $H_2/N_2$ flow, increasing the temperature linearly at a rate of 10 °C $min^{-1}$.

Textural characteristics of the catalysts were determined from nitrogen adsorption isotherms at −196 °C using an Autosorb IQ – Quantachrome instrument. The samples (*ca.* 200 mg) were degassed for 2 hours at 300 °C before the analysis. Specific surface areas were determined by the Brunauer–Emmett–Teller method from the adsorption isotherms in a relative pressure range $0.07 < P/P_o < 0.3$. The total pore volume of the amount of $N_2$ adsorbed at a relative pressure close to unity was obtained. The average pore diameter was determined by the Barrett–Joyner–Halenda method from the $N_2$ desorption isotherms.

Micro-Raman spectra were collected using a Horiba LABRAM-HR spectrometer. Measurements were performed by using a helium–neon laser (632.8 nm and an effective power of 6 mW at the sample's surface) equipped with diffraction gratings of 600 and 1800 grooves $mm^{-1}$, a Peltier-cooled CCD detector, a confocal Olympus microscope (100× objective), and an experimental resolution of typically 1 $cm^{-1}$ for 10 accumulations of 20 s.

The structure and morphology of the samples were verified by transmission electron microscopy (TEM) and high-resolution transmission electron microscopy (HRTEM) (Jeol, model 3010, operated at 300 KV) equipped with X-ray energy dispersive spectroscopy.

### 2.2. Catalytic oxidation experiments

The catalytic oxidation of the α-bisabolol (**1**) was carried out in a glass reactor equipped with a magnetic stirrer. In a typical run, a mixture of α-bisabolol (5 mL, 0.5 mol $L^{-1}$), carvyl acetate (internal standard, 0.05 mol $L^{-1}$), an aqueous solution of $H_2O_2$ (30 wt%), acetic acid (solvent) and the catalyst (0.05 g) was intensively stirred at 80 °C. The molar ratio of substrate/oxidant was 1. The products were identified and quantified by gas chromatography (GC) (Shimadzu 2014 instrument, Carbowax 20M capillary column, FID detector). Upon completion of the reaction, the catalysts were filtered off, washed with distilled water and EtOH, and reused 3 times. To control metal leaching, the catalyst was removed at the reaction temperature after 0.5 h and the solution was allowed to react further. The structures of products were confirmed by gas chromatography coupled to mass spectrometry (GC-MS) (Shimadzu QP5000 instrument, DB5 capillary column, 70 eV).

**Spectroscopic data for (2).** 2,2,6-Trimethyl-6-(4-methylcyclohex-3-en-1-yl)tetrahydro-2*H*-pyran-3-ol (bisabolol oxide A): MS (*m*/*z*/int. rel.%) 43/100; 143/45; 41/30; 93/30; 71/26; 67/24; 107/23; 125/22; 55/21; 68/20; 59/15; 79/15; 94/14; 121/13; 81/13; 238(M+)/0.3.

**Spectroscopic data for (3).** 2-(5-Methyl-5-(4-methylcyclohex-3-en-1-yl)tetrahydrofuran-2-yl)propan-2-ol (bisabolol oxide B): MS (*m*/*z*/int.rel.%) 43/100; 105/53; 143/53; 85/51; 81/45; 41/40; 93/40; 71/39; 59/38; 55/32; 119/30; 132/29; 67/28; 125/25; 161/24; 238(M+)/0.8.

## 3. Results and discussion

### 3.1. Catalyst characterization

Fig. 1 presents the XRD patterns for all catalysts with nominal compositions $CeO_2$, $Ce_{0.9}Sm_{0.10}O_{1.9-\delta}$ and $Ce_{0.85}Sm_{0.15}O_{1.9-\delta}$. The patterns show diffraction peaks corresponding to the (111), (200), (220) and (311) crystal faces, which match well with the cubic fluorite structure of $CeO_2$.[17,18] It was observed that an increase of the Sm content decreased the phase crystallinity through the broadening of the diffraction peaks together with the formation of smaller nanoparticles.[13,18] The crystallite size of the catalysts ($D$) was estimated from the (111) diffraction peak by the Scherrer equation:

$$D = 0.90\lambda/\beta_{1/2} \cdot \cos\theta \quad (1)$$

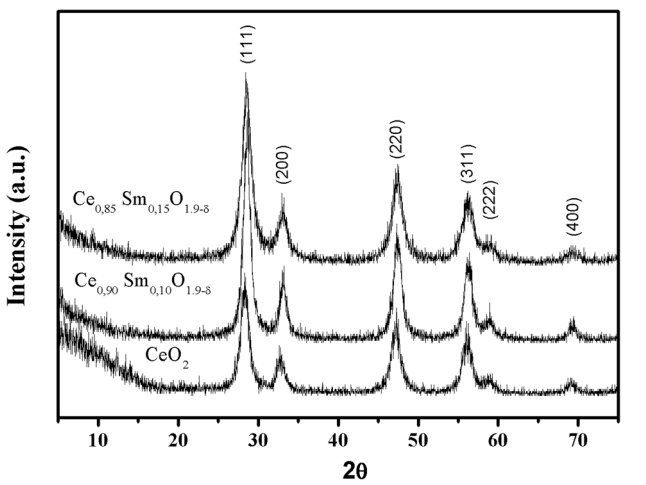


Fig. 1 XRD patterns of $CeO_2$, $Ce_{0.90}Sm_{0.10}O_{1.9-\delta}$ and $Ce_{0.85}Sm_{0.15}O_{1.85-\delta}$.

where $\lambda$ is the wavelength for $CuK_{\alpha 1}$ radiation (0.15405 nm) and $\beta_{1/2}$ is the full width at half maximum of the diffraction peak. It was observed that the $CeO_2$, $Ce_{0.90}Sm_{0.10}O_{1.9-\delta}$ and $Ce_{0.85}Sm_{0.15}O_{1.9-\delta}$ catalysts showed average crystallite sizes of 8.1, 7.6 and 7.2 nm, respectively. It is expected that this decrease in the particle size would influence directly the catalytic behavior of these materials,[19] which will be discussed later. Moreover, the absence of diffraction peaks of $Sm_2O_3$ suggests the incorporation of this lanthanide into the $CeO_2$ matrix occurring as a solid solution.[20]

The determination of reducible species present on the catalyst surface and the temperature at which these species are reduced give important information that can help us to clarify the catalytic performances observed.[20] Fig. 2 shows the TPR profiles of the $CeO_2$, $Ce_{0.9}Sm_{0.1}O_{1.9-\delta}$ and $Ce_{0.85}Sm_{0.15}O_{1.9-\delta}$ catalysts. According to the literature,[20–23] the TPR spectrum of $CeO_2$ may contain between one and three peaks. The first peak, in the temperature range 400–550 °C, is usually ascribed to the reduction of the ceria surface (the reduction of the outermost layer of $Ce^{4+}$ produced at low temperature). The second peak, between 600 and 650 °C, could be due to the formation of non-stoichiometric oxides of composition $Ce_yO_x$, while the third peak (occurring at temperatures higher than 800 °C) would indicate the reduction of $CeO_2$ to $Ce_2O_3$ in the bulk. These $H_2$ consumption peaks centered above 800 °C are generally attributed to the reduction of $CeO_2$ due to the movement of oxygen anions through vacancies[19,20] or due to the presence of $CeO_2$ nanoparticles in the fluorite lattice of the doped oxide.[20,22,24] The vacancies are introduced in the oxygen sublattice to balance the effective negative charge of the dopant cations.[22,24,25] Nevertheless, the TPR peak at the highest temperature could also indicate the reduction of $CeO_2$ to $CeO_{2-\delta}$.[26]

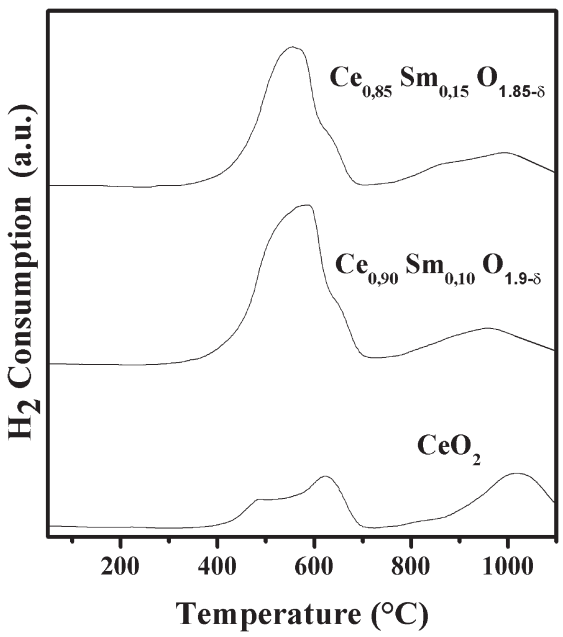


Fig. 2 $H_2$-TPR profiles of $CeO_2$, $Ce_{0.90}Sm_{0.10}O_{1.9-\delta}$ and $Ce_{0.85}Sm_{0.15}O_{1.9-\delta}$.

In this work, the TPR profile of the pure $CeO_2$ sample shows three peaks with maxima at around 500, 650 and 1000 °C. These peaks are attributed to the reduction of surface and bulk ceria, as discussed above. Sm doping caused a modification in the TPR profiles of the samples, as can be seen in Fig. 2.

The reduction peaks, in terms of peak shape, intensity and position, present differences which indicate that the catalyst reducibility is affected by the samarium addition. Intense reduction peaks at around 580 °C and 600 °C for $Ce_{0.85}Sm_{0.15}O_{1.9-\delta}$ and $Ce_{0.90}Sm_{0.10}O_{1.9-\delta}$ catalysts, respectively, as well as a broadening of the peaks located at high temperature were observed. This phenomenon could indicate that the amount of surface oxygen of ceria increases due to the diffusion of bulk oxygen to the surface as the Sm content increases.

It is interesting to note that the TPR profiles of the samples show that the reduction peaks shift to lower temperatures as the Sm content increases. It has been found that the higher the lanthanide oxide dispersion and the smaller the particle size, the lower the reduction peak temperature of the metal oxide in the TPR pattern.[27,28] The position and intensity of the hydrogen consumption peaks could also indicate the surface oxygen mobility of some oxides, such as $CeO_2$. The surface oxygen mobility increase can be associated with the decrease in the temperature at which the reduction peak appears. This fact should be attributed to the decrease in the crystallite size of the sample; thus, in our case, the surface oxygen species became more active from $Ce_{0.90}Sm_{0.10}O_{1.9-\delta}$ to the $Ce_{0.85}Sm_{0.15}O_{1.9-\delta}$ sample. This implies that the $Ce_{0.85}Sm_{0.15}O_{1.9-\delta}$ catalyst can exhibit a higher oxygen mobility.[29,30] These results are consistent with our previous results and indicate that the decrease of the particle sizes due to Sm doping allows the reduction of ceria at lower temperatures and the occurrence of higher mobility of oxygen anions in the fluorite lattice.

Raman spectra of the $CeO_2$, $Ce_{0.9}Sm_{0.1}O_{1.9-\delta}$ and $Ce_{0.85}Sm_{0.15}O_{1.9-\delta}$ catalysts are shown in Fig. 3a. The spectrum of pure $CeO_2$ is dominated by a strong band at 467 $cm^{-1}$, which is attributed to the symmetric stretching vibration of the oxygen atoms around $Ce^{4+}$ ions ($F_{2g}$ mode of the fluorite-type structure).[31] For the doped catalysts, the $F_{2g}$ mode appears at lower wavenumbers (463 and 461 $cm^{-1}$, respectively, for 10% Sm and 15% Sm) since the ionic radius of $Sm^{+3}$ (0.108 nm) is larger than that of $Ce^{+4}$ (0.097 nm). The substitution of $Ce^{+4}$ by $Sm^{+3}$ will cause an expansion of the lattice, thus reducing the wavenumbers as expected.[32] The Raman spectra of Sm-doped samples also show two broad bands around 550 and 600 $cm^{-1}$ (see Fig. 3b). The band at 600 $cm^{-1}$ is ascribed to the intrinsic oxygen vacancies due to the presence of $Ce^{+3}$. The band near 550 $cm^{-1}$ could be assigned to oxygen vacancies introduced into the ceria in order to maintain charge neutrality when $Ce^{+4}$ ions are replaced by trivalent Sm ions.[32] Another mode was observed for Sm-doped catalysts at 1060 $cm^{-1}$ and could be assigned to the presence of carbonates probably due to atmospheric contamination.[33]

 

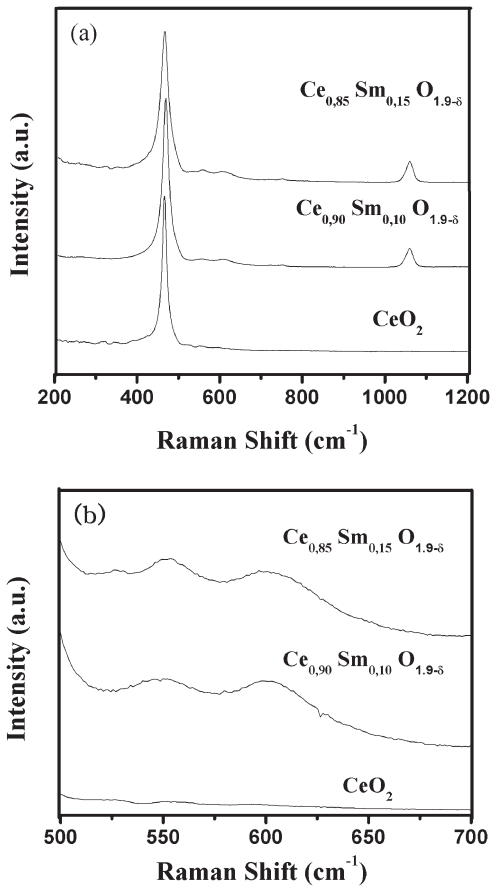


Fig. 3 Raman spectra of $CeO_2$, $Ce_{0.9}Sm_{0.1}O_{1.9-\delta}$ and $Ce_{0.85}Sm_{0.15}O_{1.85-\delta}$: (a) full spectra and (b) zoom at 500–700 $cm^{-1}$.

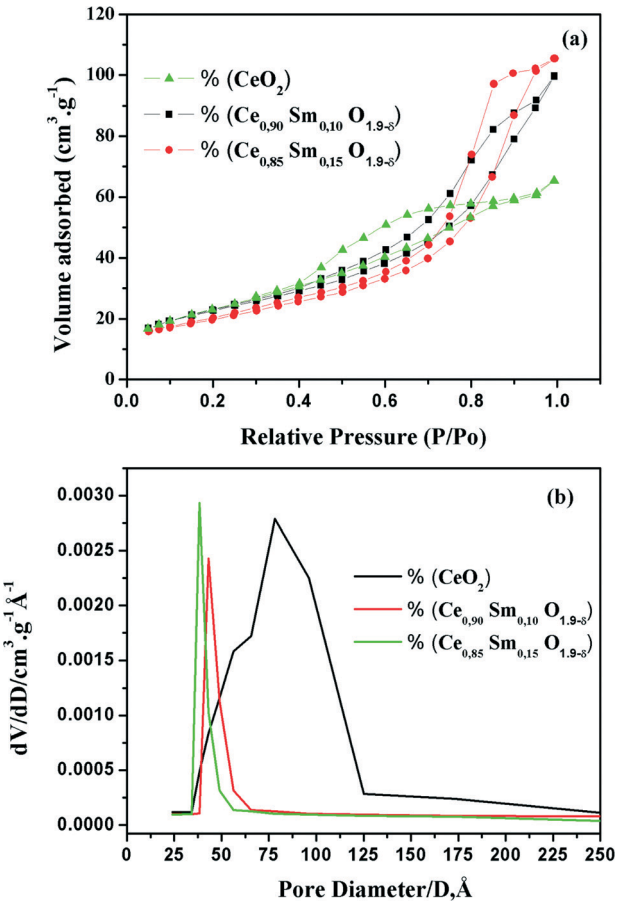


Fig. 4 Textural characterization of catalysts: (a) $N_2$-adsorption isotherms and (b) pore size distribution curves obtained using the BJH method from $N_2$ desorption isotherms.

Our results indicate that doping ceria with Sm lead to stable solid solutions but increase the content of oxygen vacancies in the bulk. It is well known that more defective structures exhibit larger mobile oxygen species contents.[34] In our case, the doped samples, which exhibit the smallest crystal sizes, show a larger amount of crystalline defects compared to undoped ceria. These results are in agreement with XRD and TPR analyses.

Table 1 shows the textural characteristics of the catalysts measured by $N_2$ physisorption. Fig. 4a shows the $N_2$ adsorption–desorption isotherms and their respective BJH pore size distribution (Fig. 4b). The catalysts showed values of the specific surface area between 75–119 $m^2\ g^{-1}$, decreasing in the following order: $Ce_{0.85}Sm_{0.15}O_{1.9-\delta} > Ce_{0.90}Sm_{0.10}O_{1.9-\delta} > CeO_2$.

Also, the pore volume and size varied with increasing Sm doping (Table 1). It was observed using XRD that the doped samples present smaller particle sizes, which lead to higher specific surface areas and probably to higher oxidation activity due to more exposed active sites.

The isotherms of $CeO_2$, $Ce_{0.90}Sm_{0.10}O_{1.9-\delta}$ and $Ce_{0.85}Sm_{0.15}O_{1.9-\delta}$ catalysts correspond to type IV (IUPAC classification), which is typical of mesoporous materials (Fig. 4a). The shape of the hysteresis loop type H1 appeared at relative pressures $P/P_o \approx 0.4$ to 0.8 for $CeO_2$ and $P/P_o \approx 0.5$ to 0.9 for $Ce_{0.90}Sm_{0.10}O_{1.9-\delta}$ and $Ce_{0.85}\ Sm_{0.15}O_{1.9-\delta}$ and could be related to the formation of textural mesoporosity. The pore size distribution curves (Fig. 4b) of the $CeO_2$ catalyst showed a unimodal profile with a narrow pore size range

Table 1 Surface properties measured by $N_2$ physisorption of the catalysts

| Catalyst | Surface area ($m^2\ g^{-1}$) | Total pore volume ($cm^3\ g^{-1}$) | Average pore diameter (nm) |
|---|---|---|---|
| $CeO_2$ | 75 | 0.3 | 9.6 |
| $Ce_{0.90}Sm_{0.10}O_{1.9-\delta}$ | 108 | 0.4 | 4.2 |
| $Ce_{0.85}Sm_{0.15}O_{1.9-\delta}$ | 119 | 0.4 | 3.6 |

(3.5–12.5 nm). For the Sm-doped catalysts, even narrower pore sizes were observed: 3.5–6 nm for $Ce_{0.85}Sm_{0.15}O_{1.9-\delta}$ and 3.5–7 nm for $Ce_{0.90}Sm_{0.10}O_{1.9-\delta}$.

The morphologies of $Ce_{1-x}Sm_xO_{1.9-\delta}$ nanostructures with a cubic shape and relatively monodisperse sizes were observed by TEM (Fig. 5). The TEM images confirm that the average particle sizes are consistent with those calculated using the Scherrer equation from the XRD data.

### 3.2. Oxidation reaction performance

In this study, the catalytic activity of $Ce_{1-x}Sm_xO_{1.9-\delta}$ was evaluated in the selective oxidation of α-bisabolol using $H_2O_2$ as an oxidant in different solvents. Bisabolol oxides A and B were the main products (Scheme 1).

These compounds are naturally found in some plants, such as chamomile, but at low concentrations (lower than 2 wt%) and are widely used in the formulation of lotions, creams and cosmetics.

All reactions produced almost exclusively epoxidation products. No allylic products or allylic derivatives were detected in the reaction mixtures. In oxidation reactions using hydrogen peroxide as an oxidant catalyzed by transition metals, allylic oxidation and epoxidation are competitive processes.[35] Typically, the products of allylic oxidation are formed when the hydrogen abstraction reaction is dominant to the electrophilic attack on the double bond. In contrast to epoxidation, allylic oxidation allows to keep the double bond in the product, thus allowing subsequent functionalization. Moreover, allylic oxidation is a process involving free radicals and occurs in the presence of transition metals with low oxidation states such as $Co^{2+}$.[36,37] However, epoxidation is generally associated with metallic species with higher oxidation states.[35] The predominance of one over the other reaction is also very dependent on the terpene structure, the product nature and the relative stability of the radical allyl intermediate formed.[35,38,39]

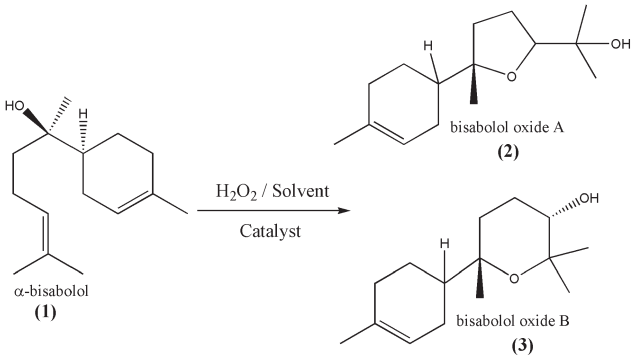


**Scheme 1** Main products obtained from oxidation of α-bisabolol catalyzed by Sm doped $CeO_2$ and pure ceria using $H_2O_2$ as an oxidant.

The influence of the reaction temperature on the oxidation of α-bisabolol catalyzed by $Ce_{0.85}Sm_{0.15}O_x$ has been studied. It was observed that the conversion of α-bisabolol increases with the increase of temperature, reaching a maximum conversion and also selectivity at 80 °C (Fig. 6). A further increase in the reaction temperature resulted in a slight decrease in the selectivity besides a significant decrease in the conversion of α-bisabolol. This result is probably due to the decomposition rate of $H_2O_2$, which is strongly temperature

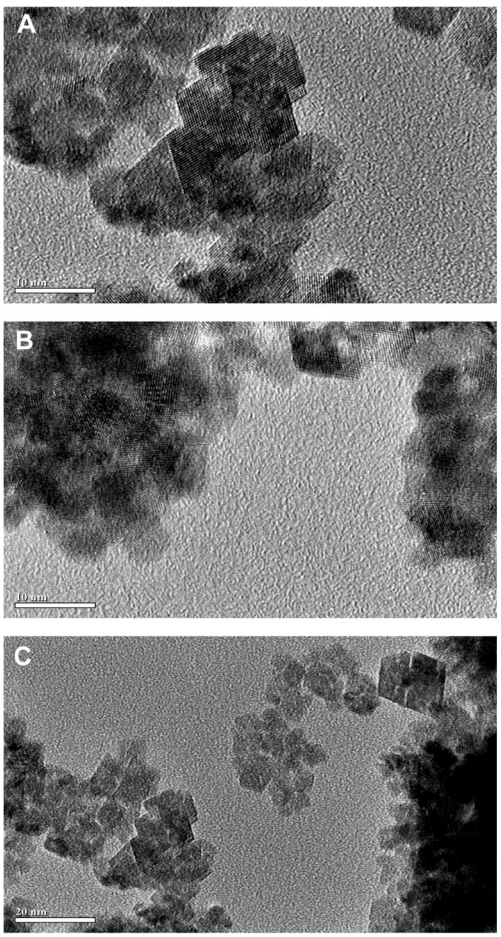


**Fig. 5** TEM images of $Ce_{1-x}Sm_xO_{1.9-\delta}$ nanoparticles: a) pure ceria, b) $Ce_{0.90}Sm_{0.10}O_{1.9-\delta}$ and c) $Ce_{0.85}Sm_{0.15}O_{1.9-\delta}$.

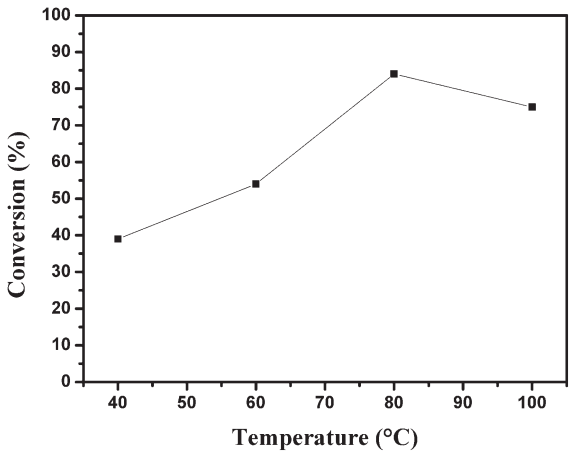


**Fig. 6** Effect of temperature on the oxidation of α-bisabolol catalyzed by $Ce_{0.85}Sm_{0.15}O_x$.

dependent. Considering the influence of the temperature on the conversion and combined selectivity of bisabolol oxides A and B, 80 °C was chosen as the most suitable temperature for the oxidation of α-bisabolol.

In a further study, we have tested different solvents for the oxidation of α-bisabolol catalyzed by Sm-containing ceria. Corma *et al.*[40] reported an increased catalytic activity in oxidation reactions with solvent polarity for both the protic and aprotic series, the increase being much more pronounced with the aprotic solvents. The positive effect of protic solvents was explained, assuming the formation of cyclic species prior to the approximation of the olefin to the metal–peroxo complex, according to the following proposed mechanism.[40] Moreover, it was reported that the product distribution can also be modified by increasing the solvent polarity for both the protic and aprotic series.[41,42] In oxidative processes, the formation of partially or totally ionic intermediates is expected and can be stabilized by polar solvents modifying significantly the selectivity for the products. Table 2 shows the effect of solvent nature on the α-bisabolol oxidation reaction catalyzed by $Ce_{1-x}Sm_xO_{1.9-\delta}$. The activities of Sm-doped ceria catalysts were observed to decrease in the order of HOAc > MeCN > MeCOMe as a result of decreasing solvent polarity. As expected, a significant modification of the product distribution is observed with the change in the solvent. For example, for the $Ce_{0.85}Sm_{0.15}O_x$ catalyst, the molar ratio between bisabolol oxides A/B was 0.64, 0.96 and 0.46 using acetic acid, acetonitrile and acetone, respectively. Even for a conversion of 18% of α-bisabolol using acetic acid as the solvent, the molar ratio between bisabolol oxides A/B remained constant (~0.64). A possible explanation for the higher intrinsic activity of this solvent is the partial decomposition of hydrogen peroxide, which was already demonstrated to be faster in MeCN and MeCOMe than in HOAc.[43] In addition, it is known that acetic acid does not only act as a solvent because of the formation of the catalyst–peracetic acid complex when it reacts with hydrogen peroxide in the presence of metallic catalysts.[40]

The influence of $Ce_{1-x}Sm_xO_{1.9-\delta}$ catalysts on the oxidation reactions of α-bisabolol performed at 80 °C is clearly observed in Table 2. In blank reactions, low conversions and selectivities were obtained after 24 h for all solvents used. In the presence of the $CeO_2$ catalyst, a conversion of α-bisabolol of 54% after 5 hours in acetic acid with a combined selectivity of 53% for bisabolol oxides A and B was observed. However, in reactions using Sm-doped ceria catalysts, a considerable increase in the conversion of α-bisabolol and combined selectivity to bisabolol oxides A and B were observed. The $Ce_{0.90}Sm_{0.10}O_x$ catalyst showed a conversion of 78%, while the $Ce_{0.85}Sm_{0.15}O_x$ catalyst presented a conversion of 84% with 77% combined selectivity for bisabolol oxides A and B. The increasing α-bisabolol conversion observed over Sm-doped ceria catalysts could be related to their textural and bulk/surface properties. As expected,[20,22] the $Sm–O^{2-}$ vacancy interaction promotes changes in the electronic environment of the $CeO_2$ nanoparticles, resulting in a higher catalytic performance for the oxidation reaction. It has been reported that the presence of oxygen vacancies is an important factor that influences the activity of some heterogeneous catalysts improving the oxidation process.[44–46] The increase in the amount of oxygen vacancies can result in an enhancement of the bulk and surface oxygen mobility, which is believed to play an important role in oxidation reactions.[30,47–49] The higher oxygen mobility benefits the oxygen species migration across the catalyst structure, resulting in greater oxidation activity.[50]

The combination of two or more elements in a catalytic system frequently affects the oxygen mobility on its surface because of the physical–chemical interactions between them. Hence, Sm addition could influence the catalytic performances. The oxygen mobility is also associated with the catalyst reducibility. In oxidation reactions, where the catalyst is subjected to oxidation–reduction cycles, its behavior can be correlated with the oxide reducibility and both reduction and reoxidation are affected by the oxygen mobility of the catalyst.[48,51] The order of catalytic activity obtained in this work is as follows: $Ce_{0.85}Sm_{0.15}O_{1.9-\delta} > Ce_{0.90}Sm_{0.10}O_{1.9-\delta} > CeO_2$. It is interesting to note, from our DRX, TPR and Raman data, that the Sm addition resulted in a decrease in the particle size

**Table 2** Effect of solvent and samarium doping on the oxidation of α-bisabolol catalyzed by ceria[a]

| Solvent | Conv. (%) | Selectivity (%) | |
|---|---|---|---|
| | | 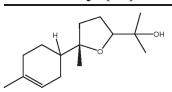 | 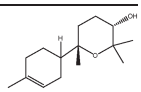 |
| Acetic acid | 17 | 2 | 4 |
| Acetonitrile | 8 | — | — |
| Acetone | 5 | — | — |
| Acetic acid | 54 | 19 | 34 |
| Acetonitrile | 17 | 18 | 21 |
| Acetone | 13 | 21 | 40 |
| Acetic acid | 78 | 23 | 38 |
| Acetonitrile | 16 | 19 | 20 |
| Acetone | 14 | 23 | 49 |
| Acetic acid | 84 | 30 | 47 |
| Acetonitrile | 19 | 22 | 23 |
| Acetone | 16 | 26 | 57 |

[a] Conditions: α-bisabolol (5 mL, 0.5 mol $L^{-1}$), carvyl acetate (internal standard, 0.05 mol $L^{-1}$), aqueous solution $H_2O_2$ (30 wt%), solvent, catalyst (0.05 g), 80 °C, 5.0 h. Conversion and selectivity were determined by GC.

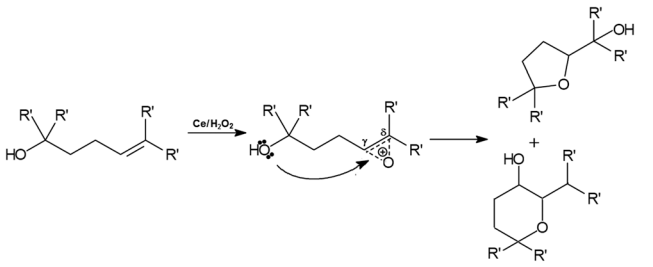


**Scheme 2** Mechanism route proposed for obtaining bisabolol oxides A and B.

Table 3 Leaching and recycle tests of $CeO_2$, $Ce_{0.90}Sm_{0.10}O_{1.9-\delta}$ and $Ce_{0.85}Sm_{0.15}O_{1.9-\delta}$ catalysts in the oxidation of α-bisabolol[a]

| | Conversion of α-bisabolol | | | |
|---|---|---|---|---|
| Catalyst | 1st recycle (%) | 2nd recycle[b] (%) | 3rd recycle[b] (%) | Leaching test[c] (%) |
| $CeO_2$ | 54 | 53 | 51 | 18 |
| $Ce_{0.90}Sm_{0.10}O_{1.9-\delta}$ | 78 | 77 | 75 | 21 |
| $Ce_{0.85}Sm_{0.15}O_{1.9-\delta}$ | 84 | 84 | 83 | 26 |

[a] Conditions: α-bisabolol (5 mL, 0.5 mol $L^{-1}$), carvoile acetate (internal standard, 0.05 mol $L^{-1}$), $H_2O_2$ (30 wt%), acetic acid, catalyst (0.05 g), 80 °C, 5.0 h. Conversion and selectivity were determined by GC. [b] The catalysts were reused after each cycle. The catalysts were recovered after a simple regeneration step, removed by filtration and washed with water. [c] The catalysts were removed by filtration after 0.5 h at the reaction temperature and the filtrate was allowed to react further. No further conversion of α-bisabolol was detected after catalyst removal.

with an increase in the specific surface area, which then led to an increase in the metallic active phase dispersion, thus improving the catalytic behavior due to more exposed active sites.[52] Also, the observed increase in the amount of oxygen vacancies resulted in an increase in the oxygen mobility and the enhancement of the reducibility in the same order.

The correlation between the epoxy-selectivity and the total yield of the products may be associated with the mechanism of cerium-catalyzed epoxidation. According to the mechanism of epoxidation in alkenes catalyzed by ceria using hydrogen peroxide as an oxidant proposed by Timofeeva,[53] the major products for this reaction are the epoxide derivatives and $Ce^{4+}$ ions. These represent the Lewis acid sites that are responsible for the high activity in alkene epoxidation. The C–O bond formed in epoxidation decreases the electron density in the unsaturated carbons. Thus, the mechanism for obtaining the bisabolol oxides by heterogeneous catalysis can now be proposed through the activation of γ- and δ-carbon on the α-bisabolol molecule caused by the C–O bond formed in epoxidation that promotes a nucleophilic attack of hydroxyl on the γ- or δ-carbon leading to the formation of bisabolol oxides A or B (Scheme 2).

The leaching of cerium and samarium ions under the reaction conditions was verified in particular experiments. The catalysts were filtered off during the course of the reaction at the reaction temperature to avoid re-adsorption of the leached metal ions onto the solid support. Then, the filtrate was allowed to react further. It was verified that no further conversion of α-bisabolol was detected after catalyst removal, providing evidence in support of heterogeneous catalysis (Table 3). Thus, the reaction solution contained no significant amounts of dissolved cerium and/or samarium species and the activity of the catalyst was due to the $Ce^{4+}$ containing catalyst. The stability of the synthesized catalyst was examined by reusing the recovered catalyst after a simple regeneration step and it remained almost unaffected even after the third cycle (Table 3).

# 4. Conclusions

$Ce_{1-x}Sm_xO_{1.9-\delta}$ catalysts were successfully synthesized, characterized and tested for the liquid phase oxidation of α-bisabolol. The physicochemical properties indicated that Sm-doped ceria produces modifications in the textural and bulk/surface properties of undoped catalysts, which influence their catalytic behavior. The best performance was observed from the $Ce_{0.9}Sm_{0.15}O_{1.85-\delta}$ catalyst, probably due to its smaller nanoparticles, ease of reducibility, higher oxygen vacancy concentration, and higher oxygen mobility. The catalytic system appeared to be efficient and selective, obtaining only bisabolol oxides A and B as products. The reaction was shown to be dependent on temperature and the solvent employed. This report presents for the first time the use of heterogeneous catalysts obtained by a microwave-hydrothermal process on the oxidation of α-bisabolol.

# Acknowledgements

Financial support from CNPq, CAPES, and FAPEMIG (Brazil) is gratefully acknowledged.

# Notes and references

1 M. Besson and P. Gallezot, *Catal. Today*, 2000, **57**, 127.
2 R. Franke and H. Schilcher, *Chamomile Industrial Profiles*, T&F Group, CRC, 2005.
3 S. Petronilho, M. Maraschin, I. Delgadillo, M. A. Coimbra and S. M. Rocha, *Ind. Crops Prod.*, 2011, **34**, 1482–1490.
4 Y. Simeo and J. V. Sinisterra, *Mini-Rev. Org. Chem.*, 2009, **6**, 128–134.
5 J. Hartung, *Pure Appl. Chem.*, 2005, **77**, 1559–1574.
6 W. Zhang and H. Yamamoto, *J. Am. Chem. Soc.*, 2007, **129**, 286–287.
7 A. M. T. Silva, R. Marques and R. M. Quinta-Ferreira, *Appl. Catal., B*, 2004, **47**, 269–279.
8 D. Gamarra, C. Belver, M. Fernández-García and A. Martínez-Arias, *J. Am. Chem. Soc.*, 2007, **129**, 12064–12065.
9 S. Hilaire, X. Wang, T. Luo, R. J. Gorte and J. Wagner, *Appl. Catal., A*, 2001, **215**, 271–278.
10 C.-Y. Cao, Z.-M. Cui, C.-Q. Chen, W.-G. Song and W. Cai, *J. Phys. Chem. C*, 2010, **114**, 9865–9870.
11 N.-C. Wu, E. W. Shi, Y. Q. Zheng and W. J. Li, *J. Am. Ceram. Soc.*, 2002, **85**, 2462–2468.
12 C. Peng, Y. Wang, K. Jiang, B. Q. Bin, H. W. Liang and J. Feng, *J. Alloys Compd.*, 2003, **349**, 273–278.
13 L. Živković, V. Lair, O. Lupan and A. Ringuedé, *Thin Solid Films*, 2011, **519**, 3538–3543.

 

14 A. Pappacena, P. Porreca, M. Boaro, C. Leitenburg and A. Trovarelli, *Int. J. Hydrogen Energy*, 2012, **37**, 1698–1709.
15 Z. Gao, J. Huang, Z. Mao, C. Wang and Z. Liu, *Int. J. Hydrogen Energy*, 2011, **35**, 731–737.
16 C. Ho, J. C. Yu, T. Kwong, A. C. Mak and S. Lai, *Chem. Mater.*, 2005, **17**, 4514.
17 S. Tsunekawa, K. Ishikawa, Z. Q. Li, Y. Kawazoe and A. Kasuya, *Phys. Rev. Lett.*, 2000, **85**, 3440.
18 N. Ai, K. Chen, S. Liu, Z. Lu, W. Su and S. P. Jiang, *Mater. Res. Bull.*, 2012, **47**, 121–129.
19 N. Sutradhar, A. Sinhamahapatra, S. Pahari, M. Jayachandran, B. Subramanian, H. C. Bajaj and A. B. Panda, *J. Phys. Chem. C*, 2011, **115**, 7628–7637.
20 K. Krishna, A. Bueno-López, M. Makkee and J. A. Moulijn, *Appl. Catal., B*, 2007, **75**, 189–200.
21 N. Sutradhar, A. Sinhamahapatra, S. Pahari, M. Jayachandran, B. Subramanian, H. C. Bajaj and A. B. Panda, *J. Phys. Chem. C*, 2011, **115**, 7628–7637.
22 S. Mandala, K. K. Bando, C. Santra, S. Maity, O. O. James, D. Mehtad and B. Chowdhury, *Appl. Catal., A*, 2013, **452**, 94–104.
23 J. Y. Siang, *et al.*, *Int. J. Hydrogen Energy*, 2010, **35**, 3456–3462.
24 K. Zhou, Z. Yang and S. Yang, *Chem. Mater.*, 2007, **19**, 1215–1217.
25 P. P. Dholabhai and J. B. Adams, *J. Mater. Sci.*, 2012, **47**, 7530–7541.
26 J. P. Holgado, R. Alvarez and G. Munera, *Appl. Surf. Sci.*, 2000, **16**, 301–315.
27 M. Kang, M. W. Song and C. H. Lee, *Appl. Catal., A*, 2003, **251**, 143–156.
28 I. I. Soykal, H. Sohn and U. S. Ozkan, *ACS Catal.*, 2012, **2**, 2335–2348.
29 E. Mamontov and T. Egami, *J. Phys. Chem. B*, 2000, **104**, 11110–11116.
30 G. B. Sun, K. Hidajat, X. S. Wu and S. Kawi, *Appl. Catal., B*, 2008, **81**, 303–312.
31 M. Teng, L. Luo and X. Yang, *Microporous Mesoporous Mater.*, 2009, **119**, 158–164.
32 A. Nakajima, A. Yoshihara and M. Ishigame, *Phys. Rev. B: Condens. Matter Mater. Phys.*, 1994, **50**, 13297.
33 S. J. Palmer, R. L. Frost, G. Ayoko and T. Nguyen, *J. Raman Spectrosc.*, 2008, **39**, 395–401.
34 G. B. Sun, K. Hidajat, X. S. Wu and S. Kawi, *Appl. Catal., B*, 2008, **81**, 303–312.
35 R. A. Sheldon and J. K. Kochi, *Metal-catalyzed oxidations of organic compounds: mechanistic principles and synthetic methodology including biochemical processes*, Academic Press, London, 1st edn, 1981.
36 A. G. M. Silva, T. S. Rodrigues, L. V. A. Gurgel, P. A. Assis, L. F. Gil and P. A. Robles-Dutenhefner, *Ind. Crops Prod.*, 2013, **50**, 288–296.
37 E. V. Gusevskaya, P. A. Robles-Dutenhefner and V. M. S. Ferreira, *Appl. Catal., A*, 1998, **174**, 177–186.
38 L. Menini, M. J. Silva, M. F. F. Lelis, J. D. Fabris, R. M. Lago and E. V. Gusevskaya, *Appl. Catal., A*, 2004, **269**, 117–121.
39 L. Menini, M. C. Pereira, L. A. Parreira, J. D. Fabris and E. V. Gusevskaya, *J. Catal.*, 2008, **254**, 355–364.
40 A. Corma, P. Esteve and A. Martínez, *J. Catal.*, 1996, **161**, 11–19.
41 V. V. Costa, L. F. Sousa, K. A. S. Rocha, P. A. Robles-Dutenhfner and E. V. Gusevskaya, *J. Mol. Catal. A: Chem.*, 2011, **235**, 72–77.
42 M. Silva, P. A. Robles-Dutenhfner, L. Menini and E. V. Gusevskaya, *J. Mol. Catal. A: Chem.*, 2003, **201**, 71–77.
43 W. Yao, Y. Chen, L. Min, H. Fang, Z. Yan, H. Wang and J. Wang, *J. Mol. Catal. A: Chem.*, 2006, **246**, 162–166.
44 S. Todorova, A. Naydenov, H. Kolev, J. P. Holgado, G. Ivanov, G. Kadinov and A. Caballero, *Appl. Catal., A*, 2012, **413–414**, 43–51.
45 Z.-Y. Tian, P. H. T. Ngamou, V. Vannier, K. Kohse-Höinghaus and N. Bahlawane, *Appl. Catal., B*, 2012, **117–118**, 125–134.
46 J.-Y. Luo, M. Meng, X. Li, X.-G. Li, Y.-Q. Zha, T.-D. Hu, Y.-N. Xie and J. Zhang, *J. Catal.*, 2008, **254**, 310–324.
47 C. Zhang, S. Li, M. Li, S. Wang, X. Ma and J. Gong, *AIChE J.*, 2012, **58**, 516–525.
48 I. I. Soykal, B. Bayram, H. Sohn, P. Gawade, J. T. Miller and U. S. Ozkan, *Appl. Catal., A*, 2012, **449**, 47–58.
49 L. F. Liotta, G. Di Carlo, G. Pantaleo and G. Deganello, *Catal. Commun.*, 2005, **6**, 329–336.
50 H. Song and U. S. Ozkan, *J. Catal.*, 2009, **261**, 66–74.
51 S. Todorova, G. Kadinov, K. Tenchev, A. Caballero, J. P. Holgado and R. Pereñíguez, *Catal. Lett.*, 2009, **129**, 149–155.
52 A. G. M. Silva, P. A. Robles-Dutenhefner, A. Dias, H. V. Fajardo, A. S. P. Lovón, J. J. Lovón-Quintana and G. P. Valença, *J. Sol-Gel Sci. Technol.*, 2013, **67**, 273–281.
53 M. N. Timofeeva, S. H. Jhung, Y. K. Hwang, D. K. Kim, V. N. Panchenko, M. S. Melgunov, Yu. A. Chesalov and J.-S. Chang, *Appl. Catal., A*, 2007, **317**, 1–10.